Clinical Neurophysiology 193 (2027) 2112427

Contents lists available at ScienceDirect

Clinical Neurophysiology

journal homepage: www.elsevier.com/locate/clinph

Individualized TMS–EEG mapping reveals clinically relevant early prefrontal cortical activity in major depressive disorder

Elena Ukharova [a,b], Isabella O'Meeghan [a], Ida Granö [a], Sabin Sathyan [a], Emi Iizuka [a], Casper Tillander [a], Noora Kainulainen [a], Maercio Maia Alves [a], Melina Engelhardt [a], Paula Partanen [d,e], Maria Vesterinen [a,e], Satu Palva [e,j], J.Matias Palva [a,e], Timo Roine [a], Juha Gogulski [a,i], Zafiris J. Daskalakis [f], Daniel M. Blumberger [g,h], Risto J. Ilmoniemi [a,c], Pantelis Lioumis [a,c,i,*]

[a] Department of Neuroscience and Biomedical Engineering, Aalto University School of Science, Espoo, Finland
[b] Department of Clinical Neurophysiology, HUS Diagnostic Center, Helsinki University Hospital and University of Helsinki, Helsinki, Finland
[c] BioMag Laboratory, HUS Medical Imaging Center, Aalto University, University of Helsinki and Helsinki University Hospital, Helsinki, Finland
[d] Division of Psychology, VISE, Faculty of Education and Psychology, University of Oulu, Finland
[e] Neuroscience Center, Helsinki Institute of Life Science, University of Helsinki, Finland
[f] Department of Psychiatry, University of California San Diego, San Diego, California, United States
[g] Temerty Centre for Therapeutic Brain Intervention, Centre for Addiction and Mental Health, Canada
[h] Department of Psychiatry, Temerty Faculty of Medicine, University of Toronto, Canada
[i] Cognitive Brain Research Unit, Department of Psychology and Logopedics, Faculty of Medicine, University of Helsinki, Helsinki, Finland
[j] School of Psychology and Neuroscience, University of Glasgow, Glasgow, United Kingdom

ARTICLE INFO

Keywords:
Major depressive disorder
Transcranial magnetic stimulation
TMS–EEG
Dorsolateral prefrontal cortex
Cortical excitability

ABSTRACT

Objective: To determine whether individualized TMS–EEG mapping improves assessment of early cortical responses in the dorsolateral prefrontal cortex (DLPFC) compared with conventional Beam F3 targeting and their association with depressive symptom severity.
Methods: Single-pulse TMS–EEG was performed in 30 patients with major depressive disorder (MDD) and 15 healthy controls. Individualized mapping identified DLPFC stimulation sites and intensities that minimized artifacts while eliciting robust early TMS-evoked potentials (>6 μV within 60 ms). Responses were compared with Beam F3 stimulation at 120% resting motor threshold. Early cortical activity was quantified using global mean field power (GMFP) and region-of-interest (ROI) area-under-the-curve (AUC) during the 10–30 ms post-stimulation interval.
Results: Individualized mapping produced distinct early cortical responses and significantly smaller early GMFP and ROI AUC responses ($q < 0.001$) compared to Beam F3 stimulation. Within the MDD group, lower GMFP AUC was associated with greater depression (PHQ-9: $\rho = -0.43$, $q = 0.046$) and anxiety severity (GAD-7: $\rho = -0.58$, $q = 0.008$). Lower ROI AUC was associated with greater depressive symptoms (PHQ-9: $\rho = -0.57$, $q = 0.008$; QIDS-SR: $\rho = -0.48$, $q = 0.033$) and anxiety severity (GAD-7: $\rho = -0.45$, $q = 0.040$). No significant clinical associations were observed for Beam F3-derived measures.
Conclusions: Individualized TMS–EEG mapping identifies clinically relevant early DLPFC responses not detected using conventional Beam F3 targeting.
Significance: Individualized targeting improves the sensitivity of prefrontal TMS–EEG and may enhance detection of early cortical responses associated with depressive and anxiety severity.

1. Introduction

Currently, depression is diagnosed largely on the basis of subjective symptom questionnaires and clinical interviews. Despite more than 20 pharmacological and non-pharmacological interventions approved for MDD, many patients undergo a long course of trial and error, possibly

* Corresponding author at: Department of Neuroscience and Biomedical Engineering, Aalto University School of Science, Espoo, Finland.
E-mail address: pantelis.lioumis@aalto.fi (P. Lioumis).

https://doi.org/10.1016/j.clinph.2026.2112427
Accepted 29 September 2026
Available online 1 October 2026
1388-2457/© 2026 The Authors. Published by Elsevier B.V. on behalf of International Federation of Clinical Neurophysiology. This is an open access article under the CC BY license (http://creativecommons.org/licenses/by/4.0/).

leading to significant delays in achieving treatment response and remission (Leuchter et al., 2009). Fewer than 50% of individuals with depression respond to the first antidepressant, and only 30% achieve full remission (Trivedi et al., 2006). Consequently, there is a pressing need for objective neurophysiological biomarkers that can guide treatment selection and facilitate personalized interventions.

Concurrent TMS and EEG (TMS–EEG) enables direct evaluation of cortical properties, showing promise as a tool for identification of biomarkers of psychiatric conditions (Cao et al., 2021; Kallioniemi and Daskalakis, 2022; Sun et al., 2016). Changes in TMS-evoked potentials (TEPs) have been linked to depression diagnosis and symptom severity. When stimulating the left dorsolateral prefrontal cortex (DLPFC), MDD patients show larger amplitudes of peaks occurring at 45, 60, and 100 ms post-stimulus, referred to as N45, P60, and N100, than in healthy controls (Voineskos et al., 2019). Additionally, P60 and N100 amplitudes have been correlated with depression symptom severity (Cash et al., 2021; Fox et al., 2012; Li et al., 2021; Weigand et al., 2018). Increased cortical excitation has also been reported, evidenced by increased global mean field amplitude area under the curve (GMFA–AUC) (Voineskos et al., 2019). Furthermore, P30, N45, P60, and N100 amplitudes have been shown to predict the degree of treatment response to theta-burst stimulation (Dhami et al., 2023), repetitive TMS (rTMS; Eshel et al., 2020) and magnetic seizure therapy (MST) (Sun et al., 2016).

Despite these promising findings, several methodological limitations constrain the reproducibility and interpretability of TEP-based biomarkers. Early (<60 ms) TEP components that are considered to reflect local cortical reactivity (Casarotto et al., 2022; Ilmoniemi et al., 1997) may be obscured by artifacts, and thus, their assessment demands individualized targeting and rigorous artifact control. Conversely, the later components are less specific to cortical excitability and may include auditory and somatosensory confounds (Conde et al., 2019; Hernandez-Pavon et al., 2023; Tremblay et al., 2019). Additionally, the early TEP components are connected to the local NMDA- and GABA-A-mediated activity and may index local excitation/inhibition balance (Darmani and Ziemann, 2019).

Previous work on TMS–EEG biomarkers in depression has relied on Talairach (Voineskos et al., 2019) or MNI coordinates (Dhami et al., 2023, 2020) and EEG electrode positions (Biermann et al., 2022; Sun et al., 2016). These methods, despite standardised methodology, neglect the effect of interindividual differences in head anatomy, scalp-to-cortex distance, cortical morphology, and gyrification. Scalp-based methods can deviate by up to 2 cm from individual MRI-defined DLPFC targets (Ahdab et al., 2010). Furthermore, anatomical correspondence does not guarantee functional correspondence due to interindividual variability in structure–function relationships (Casali et al., 2010). Additionally, previous work has utilized fixed coil orientations (Biermann et al., 2022; Dhami et al., 2023, 2020; Sun et al., 2016; Voineskos et al., 2019), disregarding individual differences in gyral morphology of the DLPFC.

Likewise, stimulation intensity is typically defined relative to the resting motor threshold (RMT), without accounting for individual differences in anatomy or cortical reactivity (Biermann et al., 2022; Dhami et al., 2023, 2020; Sun et al., 2016; Voineskos et al., 2019). However, electric-field (E-field) modeling and monitoring reveal large inter-individual differences in cortical dosing at a given RMT defined by stimulator output. Consequently, conventional 120% RMT dosing risks substantial over- or under-stimulation, underscoring the need for individualized E-field monitoring (Caulfield et al., 2021).

Together, these factors may contribute to variability in TEP measurements and limit the sensitivity of proposed biomarkers. To address these challenges, we developed an individualized TMS–EEG mapping procedure that integrates anatomical information, functional connectivity, coil orientation, stimulation intensity, and real-time electrophysiological feedback to identify DLPFC stimulation parameters that maximize the detectability of early cortical responses while minimizing artifacts (Ukharova et al., 2025).

The present study focused on early TEP responses following stimulation of the left DLPFC. First, we compared conventional Beam F3 targeting (Beam et al., 2009) with individualized TMS–EEG mapping to determine how stimulation target selection influences the quantification of early cortical responses. Because individualized mapping was designed to maximize early cortical activation (Casarotto et al., 2022), we expected it to alter the temporal profile of the TMS-evoked response relative to conventional targeting. To assess whether any observed differences could be explained by non-neural activity, we additionally quantified the early TMS-induced muscle artifact for both targeting approaches.

To characterize early cortical activity, we evaluated conventional TEP peak amplitudes together with area-under-the-curve (AUC) measures of global mean field power (GMFP) and the left DLPFC region-of-interest (ROI) waveform. AUC measures quantify activity across predefined time windows, providing a peak-independent characterization of the evoked response that is less sensitive to variability in peak identification and waveform morphology than conventional peak-based metrics. We hypothesized that these measures would provide a more robust characterization of early cortical responses and their relationship to clinical symptoms.

After establishing the effects of stimulation targeting, we compared TEP responses of participants with major depressive disorder (MDD) and healthy controls. Finally, we examined associations between TMS–EEG measures and symptom severity within the MDD group using the Patient Health Questionnaire (PHQ-9), Quick Inventory of Depressive Symptomatology (QIDS-SR), and Generalized Anxiety Disorder scale (GAD-7). We expected that MDD would be associated with alterations in the temporal distribution of early cortical activity and that these measures would be associated with greater symptom severity.

2. Methods

Detailed study procedures have been described previously in Ukharova et al. (2025).

2.1. Participants

30 MDD patients and 15 healthy controls (demographics, comorbidities, and medication statuses are presented in Table 1) were recruited from the participant pool of the larger PlaStim (Plasticity Stimulation in the Treatment of Anhedonia) study of Wellcome Leap Multichannel Psych Program (CA, USA). The sample size discrepancy reflected prioritization of clinical data collection within project timelines. The study was approved by the Helsinki University Hospital Ethics Committee (HUS/3043/2021). Written informed consent was obtained from all participants.

Inclusion criteria for all participants were: Age 18–65, no contraindication for MRI, not pregnant or nursing, no neurological disorders such as epilepsy or brain injury.

For MDD patients additional inclusion criteria were: current major depressive episode (MINI score ≥5, assessed by a clinical coordinator), no acute suicide risk, no history of psychosis, no forensic or disability status.

For healthy subjects, exclusion criteria entailed: any psychiatric disorder diagnosis (assessed with MINI questionnaire), and use of substances that affect the central nervous system (other than alcohol or nicotine products).

2.2. MRI acquisition

MRI data were acquired using a MAGNETOM Skyra 3 T scanner (Siemens Healthcare GmbH, Erlangen, Germany) with a 32-channel head coil, including T1-weighted structural imaging, resting-state fMRI, and diffusion-weighted imaging (DWI).

Table 1
Data shown for MDD (30) and healthy (15) subjects, showing mean score and standard deviation. Abbreviations: BPD, Borderline Personality Disorder, ADHD, Attention Deficit Hyperactivity Disorder, ADD, Attention Deficit Disorder, PTSD, Post-Traumatic Stress Disorder, OCD, Obsessive–Compulsive Disorder, QIDS-SR, Quick Inventory of Depressive Symptomatology Self-Report; RRS, Ruminative Response Scale; PHQ, Patient Health Questionnaire; GAD-7, Generalized Anxiety Disorder scale.

	MDD ($N = 30$)	Healthy ($N = 15$)
Age	34 ± 10	28 ± 4
Gender		
Male	15	10
Female	12	5
Other	2	–
Trans	1	–
Other diagnoses		
Anxiety	15	–
Social anxiety	2	–
BPD	4	–
Panic disorderADHD	34	–
(ADD)	(1)	–
Autism	3	–
PTSD	3	–
OCD	1	–
Medication status		
None	9	15
SSRI	5	–
SNRI	4	–
Tricyclic	1	–
Vortioxetine	5	–
Bupropion	1	–
Other	3	–
Unknown	3	–
Symptom Scores (Mean + SD)		
QIDS-SR	13 ± 4	3 ± 3
RRS	18 ± 3	11 ± 5
PHQ	14 ± 6	2 ± 1
GAD-7	9 ± 5	1 ± 2

.

2.2.1. T1-weighted structural imaging

T1-weighted anatomical images were obtained using a magnetization-prepared rapid gradient echo (MPRAGE) sequence (see full parameters in Supplementary Methods).

Images were processed with *FreeSurfer* to obtain cortical surfaces and subject-specific parcellations. The HCP-MMP1.0 atlas (Glasser et al., 2016) was projected to individual anatomy to define cortical and subcortical ROIs.

2.2.2. Resting-state functional MRI

Resting-state functional MRI (rs-fMRI) data were collected using a T2*-weighted gradient-echo echo-planar imaging (EPI) sequence (see full parameters in Supplementary Methods) and preprocessed with *fMRIPrep* (Esteban et al., 2019) (motion and distortion correction, T1 coregistration), followed by the removal of initial volumes, denoising with motion/physiological confounds, 0.01–0.08 Hz temporal filtering, and 6-mm smoothing. Seed-to-voxel connectivity was computed using Pearson correlations (Fisher z-transformed).

2.2.3. Diffusion-weighted imaging

Diffusion-weighted imaging (DWI) was acquired using a single-shot spin-echo EPI sequence (see full parameters in Supplementary Methods) and preprocessed using the PyDesigner pipeline (Dhiman et al., 2024), including noise, motion, eddy-current, Gibbs, and distortion correction. Fiber orientation distributions were estimated with multi-tissue CSD and aligned to T1 space using *MRtrix3* (Tournier et al., 2019). Anatomically constrained tractography priors were derived from FreeSurfer segmentations. Real-time tractography performed with *rttvis* (Aydogan et al., 2023) was used to identify stimulation-relevant regions, prioritizing either widespread structural connectivity or dense streamline projections to network-relevant targets.

2.3. EEG recording

EEG was measured with a 62-channel cap (EasyCap, Germany) with Ag/AgCl sintered electrodes connected to a TMS-compatible EEG amplifier (Brain Products, Gmbh, Germany). Signals were low-pass filtered with a 1000-Hz cut-off frequency and sampled at 5000 Hz. Reference and ground electrodes were placed on the right mastoid and right zygomatic bone.

2.4. TMS protocol

TMS was applied with a 70-mm radius figure-of-eight coil attached to a TMS stimulator (NBT 2.2.4, Nexstim Ltd., Finland) with an integrated MRI-guided neuronavigation and EMG.

2.4.1. Resting motor threshold

RMT was determined from right abductor pollicis brevis (APB) motor-evoked potentials using maximum-likelihood algorithm (Awiszus, 2003).

2.4.2. Minimizing auditory responses to TMS

Auditory responses were minimized using auditory masking (Russo et al., 2022) delivered through hybrid earplugs and earphones (ER3C Insert Earphones, Etymotic Research Inc., IL, USA).

2.4.3. Target and stimulation parameters selection

For each subject, two TMS stimulation targets were selected: a standardised LDLPFC target using Beam F3 (Beam et al., 2009), and an individualised target identified through TMS–EEG mapping using individual brain connectivity and responses to TMS stimulation.

2.4.4. Standardised target

Beam F3 approximates the location of the DLPFC based on head circumference, nasion–inion distance, and left tragus to right tragus distance (Beam et al., 2009). The stimulation target was set based on these three measurements with a coil orientation of 45 degrees to the midline and stimulation intensity of 120% of the RMT (Beam et al., 2009), except 2 subjects, for whom the stimulation was delivered at 105% RMT due to discomfort and pain tolerance.

2.4.5. Individualised target

The full procedure of individualized target identification mapping is described in detail in our recent study (Ukharova et al., 2025) and summarized in Fig. 1. In brief, T1 MRIs and resting state fMRI were used to create individualized region of interest (ROI) maps, based on the functional anticorrelation between LDLPFC and sgACC (Cash et al., 2021; Cash and Zalesky, 2024; Cole et al., 2020; Fox et al., 2012). The resulting maps were then overlaid on the individual MRI in the neuronavigation software. This ROI served as a guide for the TMS–EEG target mapping procedure prior to selecting the stimulation target within the LDLPFC (Fig. 1A). The candidate targets were additionally investigated using real-time tractography (Aydogan et al., 2023), priority given to the cortical sites with widespread or MDD network-specific structural connectivity (Siddiqi et al., 2021).

The coil was initially placed over one of the areas displaying the highest functional anticorrelation with sgACC within the LDLPFC, in the posterior-anterior direction of the induced electric field, and stimulus intensity was set to 100–110% of RMT over this initial location. Adjustments were made based on two criteria: a) elimination of artifacts after the first 10 ms, b) a 6–10 μV peak-to-peak response of early TEP deflections (10–60 ms). If a muscle artifact was present with a duration exceeding 10 ms, the coil was rotated and/or coil position manipulated towards an artifact-free location, while staying within the LDLPFC

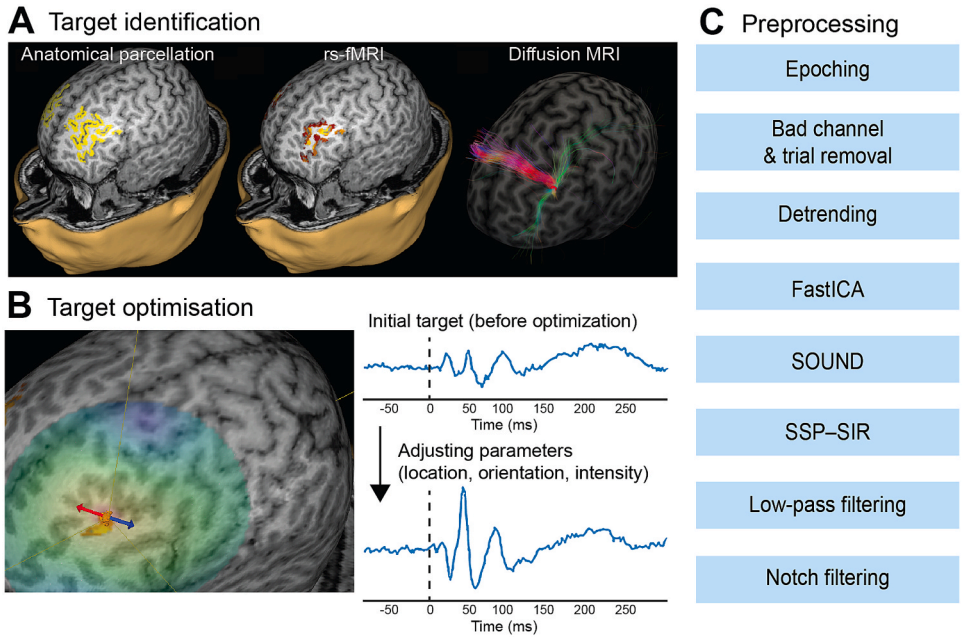


Fig. 1. Study Schematic. **(A)** Anatomic parcellations outlining the DLPFC region, resting-state fMRI highlighting the region of the DLPFC anticorrelated with the subgenual cingulate, lighter colours indicating greater anticorrelation, and diffusion MRI displaying the connectivity from the targeted area, all used to identify the initial individual stimulation sites for each subject. **(B)** Target optimization using real-time E-field and TEP visualization tools (data were baseline corrected and average referenced, TMS artifact zero-padded between −2 and 10 ms). The stimulation intensity, location, and orientation were adjusted for each subject to minimise muscle artifacts and obtain a 6–10 μV early response (10–60 ms). **(C)** The outline of the data preprocessing pipeline.

defined by the individual anatomical parcellation (for details, see (Ukharova et al., 2025)). Stimulation intensity was adjusted in 2% increments of the maximum stimulator output until the desired peak-to-peak amplitude was obtained (Supplementary Fig. 1). The final stimulation site was chosen based on both its connectivity profile and the quality of the TMS–EEG response (Lioumis and Rosanova, 2022).

2.4.6. Recordings

Prior to and during the recording, electrode impedances were kept below 5 kΩ. At each target, 300 single pulses were delivered with a jittered interstimulus interval of 2–2.3 s.

2.5. EEG data preprocessing

The recorded EEG data were preprocessed in MATLAB R2017b using the EEGLAB toolbox (Delorme and Makeig, 2004) with an automated preprocessing pipeline integrating functions from the TESA toolbox (Rogasch et al., 2017), AARATEP (Cline et al., 2021), and custom scripts. The recorded EEG signals were segmented into epochs of –1500 to 1500 ms around the TMS pulse. The TMS pulse artifact was removed by excising data from −2 to 12 ms and reconstructing the missing segment using cubic interpolation. Slow drifts were removed using robust polynomial detrending, followed by baseline correction using the interval from −500 to −5 ms.

Noisy channels were identified automatically using AARATEP and were replaced by spherical spline interpolation. Trials containing excessive artifacts were rejected automatically using robust z-score thresholds based on baseline variability, peak-to-peak amplitude, early post-stimulus root-mean-square activity, and absolute voltage. Ocular artifacts were removed with independent component analysis (FastICA) (Oja and Yuan, 2006) followed by automatic component classification with ICLabel (Pion-Tonachini et al., 2019). Noise from extracranial sources was suppressed with the source-estimate-utilizing noise-discarding algorithm (SOUND) (Mutanen et al., 2018). Any remaining TMS-evoked muscle artifacts were suppressed with signal-space projection–source-informed reconstruction (SSP–SIR) (Mutanen et al., 2016), with the number of projection components selected automatically based on residual artifact reduction while limiting overcorrection.

The data were then low-pass filtered at 80 Hz and notch filtered between 48 and 52 Hz to suppress line noise. Epochs were trimmed to the interval from −1000 to 1000 ms, rereferenced to the common average reference, and saved in EEGLAB format for subsequent analyses.

2.6. Quantification of TMS-evoked responses

Early TMS-evoked activity was quantified using area-under-the-curve (AUC) measures within the 10–30 ms post-stimulation interval. This window was selected to capture the earliest cortical response while avoiding the immediate stimulation artifact period. Early activity was quantified using two complementary signal representations: the left DLPFC region of interest (ROI) waveform, defined using electrodes AF3, F1, F3, and F5, reflecting regional response magnitude near the stimulation site, and global mean field power (GMFP), reflecting the spatially distributed magnitude of the evoked response across channels. GMFP was calculated at each time point as the spatial standard deviation of EEG amplitudes across all channels. AUC values were computed from the absolute waveform using trapezoidal integration.

To distinguish early cortical recruitment from later response activity, AUC was also quantified over the subsequent 30–80 ms interval. Clinical associations with early activity were first evaluated using Spearman rank correlations with the 10–30 ms AUC. Because stimulation intensity during individualized mapping was optimized to elicit robust early cortical responses, additional partial Spearman correlations were performed while controlling for the corresponding 30–80 ms AUC (GMFP or ROI). This analysis was used to determine whether associations with symptom severity reflected the earliest cortical response specifically rather than overall response magnitude. The 10–30 ms interval was chosen to capture the earliest cortical response, whereas the 30–80 ms interval encompassed subsequent early TEP activity while preceding the N100 component, which is more strongly influenced by auditory and somatosensory activation (Conde et al., 2019; Hernandez-Pavon et al., 2022).

For comparison with previous TMS–EEG studies, conventional TEP components were quantified from the DLPFC ROI using predefined latency windows: N15 (10–25 ms), P30 (25–40 ms), N45 (35–55 ms), P60 (50–75 ms), and N100 (80–130 ms). Negative components were defined as the minimum amplitude within the corresponding latency window, whereas positive components were defined as the maximum amplitude. Peak latencies were recorded as the time point of the identified extremum. To reduce sensitivity to differences in overall response magnitude, peak amplitudes were additionally normalized by the root-mean-square (RMS) amplitude of the ROI waveform between 10 and 80 ms.

2.7. Residual muscle artifact assessment

To assess the effectiveness of artifact suppression in both mapped and Beam F3 targets, residual TMS-evoked muscle activity was quantified using the preprocessed EEG data immediately before the final filtering stage. For each participant, time–frequency decomposition was performed on epoched data, and mean spectral power within the 30–100 Hz band was calculated over the 5–30 ms post-stimulus interval. Power values were normalized relative to the pre-stimulus −500 to −100 ms baseline and averaged across electrodes AF3, F1, F3, and F5. The resulting baseline-normalized high-frequency power served as an index of residual muscle artifact, with larger values indicating greater remaining muscle contamination following preprocessing.

2.8. Questionnaires

Depressive symptom severity was assessed using the Patient Health Questionnaire (PHQ-9). Secondary symptom measures included the Quick Inventory of Depressive Symptomatology Self-Report (QIDS-SR), and Generalized Anxiety Disorder scale (GAD-7).

2.9. Statistical analysis

All analyses were performed in Python (v3.12.11) using NumPy, Pandas, SciPy, and Statsmodels.

Group differences between participants with MDD and healthy controls were evaluated using Welch's *t*-tests and quantified using Hedges' *g* effect sizes. Because of unequal group sizes and potential deviations from normality, statistical significance was additionally assessed using permutation testing with 10,000 random label permutations. Bootstrap confidence intervals for effect sizes were estimated using 10,000 bootstrap resamples.

Paired comparisons between individualized TMS–EEG mapping and conventional Beam F3 stimulation were evaluated using paired permutation tests based on 10,000 random sign flips of within-subject differences.

Associations between TMS–EEG measures and symptom severity were assessed using Spearman rank correlations in participants with MDD. Partial Spearman correlations were additionally performed to evaluate associations between early (10–30 ms) AUC measures and symptom severity while controlling for the corresponding later (30–80 ms) AUC measure.

False discovery rate (FDR) correction using the Benjamini–Hochberg procedure was applied separately within predefined families of related hypotheses. Specifically, AUC-derived measures (GMFP and ROI) and conventional TEP measures were corrected independently for group comparisons, target comparisons, and clinical correlation analyses. Corrected P values are reported as q values.

To characterize the relationship between individualized and conventional stimulation intensities, descriptive statistics were calculated for the mapped stimulation intensity (%RMT), and its association with resting motor threshold was evaluated using Pearson correlation.

The distribution of the paired differences in the residual muscle artifact index was assessed using the Shapiro–Wilk test. As the paired differences significantly deviated from normality, residual muscle artifact between individualized LDLPFC and BeamF3 stimulation was compared using the Wilcoxon signed-rank test. Descriptive statistics are reported as median and interquartile range (IQR).

All statistical tests were two-sided, statistical significance was defined as $P < 0.05$.

3. Results

3.1. Demographics and clinical characteristics

The study sample consisted of 30 participants with MDD and 15 healthy controls. Demographic and clinical characteristics are summarized in Table 1. The MDD group included participants with a range of comorbid conditions and medication statuses.

3.2. Effect of stimulation targeting

Individualized TMS–EEG mapping produced significantly different early cortical responses compared with conventional Beam F3 stimulation (Fig. 2, Table 2). Both GMFP and ROI AUCs during the 10–30 ms interval were significantly smaller following individualized mapping than Beam F3 stimulation (GMFP: permutation $P = 0.0001$, $q = 0.0003$; ROI: permutation $P = 0.0001$, $q = 0.0003$). Similar differences were observed for the subsequent 30–80 ms interval (GMFP: $q = 0.0003$; ROI: $q = 0.0038$), indicating that stimulation target substantially influenced the magnitude of the evoked response.

Several conventional TEP measures also differed significantly between stimulation approaches after FDR correction. Beam F3 stimulation elicited larger N15 and N45 amplitudes, whereas individualized mapping produced larger P30 amplitudes and higher normalized P30 and P60 amplitudes. N45 latency was also significantly prolonged during individualized mapping (all $q < 0.05$; Table 2). Together, these findings demonstrate that individualized mapping alters both the magnitude and temporal characteristics of early DLPFC responses compared with conventional targeting.

The stimulation intensity selected during individualized mapping varied substantially across participants (mean ± SD: 117 ± 22% RMT, median 114%, range 80–213% RMT, Supplementary Table S1). Compared with the Beam F3 protocol fixed at 120% RMT, 67% of participants required lower stimulation intensities, whereas 31% required higher intensities. Furthermore, the mapped stimulation intensity expressed relative to motor threshold was strongly inversely associated with resting motor threshold ($r = -0.64$, $p < 0.001$), indicating that a fixed intensity of 120% RMT does not account for interindividual variability in prefrontal cortical responsiveness.

Residual high-frequency muscle artifact following preprocessing was significantly lower during individualized LDLPFC stimulation than during Beam F3 stimulation. The median residual muscle index was 0.50 (IQR 0.33–0.68) for individualized LDLPFC compared with 0.66 (IQR 0.47–1.43) for Beam F3 stimulation (Wilcoxon signed-rank test: $W = 211$, $p = 0.00064$). Despite identical preprocessing, individualized mapping therefore resulted in significantly lower residual muscle contamination. As cranial muscle activation occurs within the same temporal window as the earliest cortical responses, the larger early AUCs observed with Beam F3 stimulation are likely influenced, at least in part, by greater residual stimulation-related muscle activity. Together, these findings highlight the importance of optimizing stimulation site and intensity to improve the specificity of early TMS–EEG measurements.

3.3. Group differences in TMS–EEG measures

Despite clear differences between stimulation targets, early cortical activity did not differ significantly between participants with MDD and healthy controls. Neither GMFP nor ROI AUC measured during the

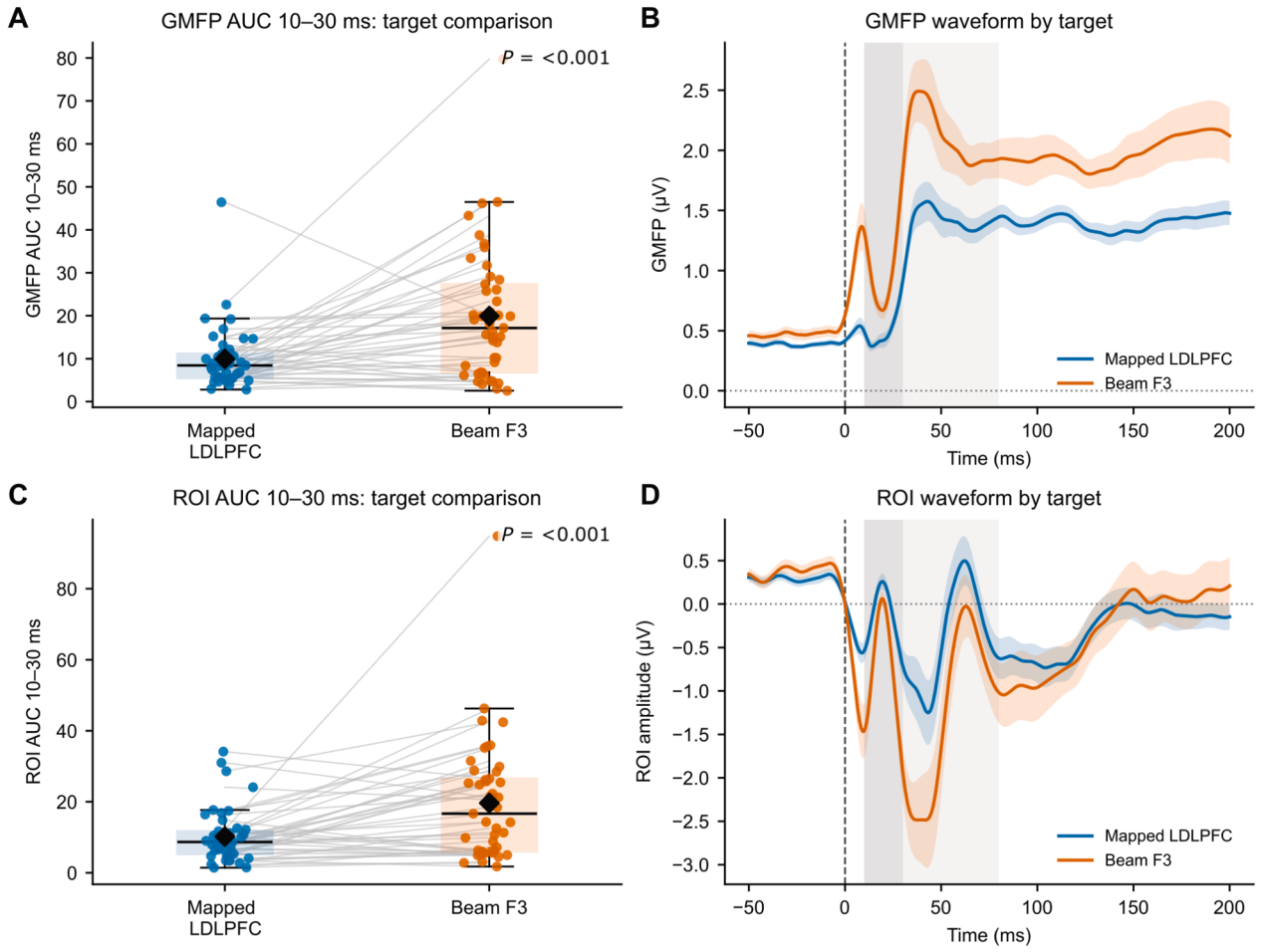


Fig. 2. Individualized TMS–EEG mapping produces distinct early cortical responses compared with conventional Beam F3 targeting. (A) Paired comparison of GMFP area under the curve (AUC) during the 10–30 ms post-stimulation interval between individualized mapped left DLPFC stimulation and conventional Beam F3 stimulation. Each point represents one participant, gray lines connect paired measurements, black diamonds indicate group means, and boxplots show the median and interquartile range. **(B)** Grand-average GMFP waveforms for mapped left DLPFC and Beam F3 stimulation. Shaded regions indicate the standard error of the mean (SEM). The gray shaded area highlights the early analysis window (10–30 ms). **(C)** Paired comparison of ROI AUC during the 10–30 ms interval for individualized mapped left DLPFC and Beam F3 stimulation. Plot elements are as described in panel A. **(D)** Grand-average ROI waveforms averaged across electrodes AF3, F1, F3, and F5 for mapped left DLPFC and Beam F3 stimulation. Shaded regions indicate SEM, and the gray shaded area denotes the 10–30 ms and 30–80 ms analysis windows.

Table 2

Comparison of early cortical response AUC measures between individualized mapped LDLPFC stimulation and conventional Beam F3 targeting. Early (10–30 ms) and later (30–80 ms) cortical activity was quantified using GMFP and ROI AUC measures. Data are presented as mean ± SD for paired observations (n = 45). Statistical significance was evaluated using paired sign-permutation tests with Benjamini–Hochberg FDR correction. Asterisks indicate statistically significant associations after FDR correction ($q < 0.05$).

Metric	n paired	Mapped LDLPFC mean ± SD	Beam F3 mean ± SD	Mapped minus Beam F3 mean difference	Hedges gz mapped minus Beam F3	Sign-permutation P	FDR q
GMFP AUC 10–30 ms	45	9.94 ± 7.19	21.43 ± 16.85	−11.49	−0.66	<0.0001	<0.0001*
ROI AUC 10–30 ms	45	10.22 ± 7.43	20.82 ± 17.63	−10.61	−0.61	<0.0001	<0.0001*
GMFP AUC 30–80 ms	45	70.35 ± 36.26	108.55 ± 61.36	−38.20	−0.60	<0.0001	<0.0001*
ROI AUC 30–80 ms	45	76.04 ± 61.64	118.63 ± 88.78	−42.59	−0.47	0.0015	0.0015*

10–30 ms interval showed significant group differences following FDR correction (GMFP: Hedges' $g = -0.42$, permutation $P = 0.178$; ROI: Hedges' $g = -0.15$, permutation $P = 0.654$; Table 3). Likewise, none of the conventional TEP amplitude or latency measures differed significantly between diagnostic groups after correction for multiple comparisons.

These findings indicate that individualized mapping primarily improved characterization of inter-individual variability rather than enhancing discrimination between diagnostic groups.

Table 3

Comparison of early cortical response AUC measures between participants with major depressive disorder (MDD) and healthy controls (HC). Group differences were evaluated for early (10–30 ms) and later (30–80 ms) cortical activity quantified using global mean field power (GMFP) and left DLPFC region-of-interest (ROI) area-under-the-curve (AUC) measures obtained during individualized mapped stimulation. Values are presented as mean ± standard deviation (SD). Statistical significance was assessed using permutation testing, and *q*-values were obtained using the Benjamini–Hochberg false discovery rate (FDR) correction applied within the AUC comparison family.

Metric	MDD n	HC n	MDD mean ± SD	HC mean ± SD	Hedges g MDD minus HC	Permutation P	FDR q within correction family
GMFP AUC 10–30 ms	30	15	8.43 ± 3.86	12.96 ± 10.82	−0.64	0.032	0.128
ROI AUC 10–30 ms	30	15	10.00 ± 6.63	10.66 ± 9.07	−0.09	0.781	0.781
GMFP AUC 30–80 ms	30	15	65.94 ± 18.60	79.17 ± 57.35	−0.36	0.279	0.558
ROI AUC 30–80 ms	30	15	72.91 ± 45.62	82.29 ± 86.99	−0.15	0.658	0.781

3.4. Early cortical activity scales with symptom severity

Clinical correlation analyses were restricted to participants with MDD (Fig. 3, Table 4). Early cortical activity measured during individualized mapping showed significant associations with symptom severity, whereas corresponding measures derived from Beam F3 stimulation showed no significant correlations.

Among the AUC measures, lower GMFP AUC during the 10–30 ms interval was associated with greater depression severity as measured by the PHQ-9 ($\rho = -0.43$, $q = 0.046$) as well as anxiety severity measured by the GAD-7 ($\rho = -0.58$, $q = 0.008$). In contrast, lower ROI AUC was associated with greater depressive symptom severity measured by the PHQ-9 ($\rho = -0.57$, $q = 0.008$) and QIDS-SR ($\rho = -0.48$, $q = 0.033$) as well as anxiety (GAD-7, $\rho = -0.45$, $q = 0.04$). No significant associations were observed for the later 30–80 ms AUC measures, and no AUC measure derived from Beam F3 stimulation correlated significantly with symptom severity after correction for multiple comparisons.

To determine whether these relationships reflected the earliest cortical response rather than overall response magnitude, partial Spearman correlations were performed while controlling for the corresponding 30–80 ms AUC (Table 5, Supplementary Fig. S2). The association between early GMFP AUC and anxiety severity remained significant after controlling for later GMFP activity (partial $\rho = -0.58$, $q = 0.003$) as well as depressive symptom severity (PHQ-9: partial $\rho = -0.43$, $q = 0.024$). Likewise, early ROI AUC remained independently associated with depressive symptom severity (PHQ-9: partial $\rho = -0.63$, $q = 0.002$) and depressive symptoms measured by the QIDS-SR (partial $\rho = -0.52$, $q = 0.008$), with a weaker independent association also observed for GAD-7 scores (partial $\rho = -0.45$, $q = 0.022$).

Among conventional TEP measures, only P60 latency showed significant clinical associations after FDR correction, correlating negatively with GAD-7 scores (Supplementary Table S3, $\rho = -0.61$, $q = 0.018$). No other canonical TEP amplitude or latency measures remained significant after correction for multiple comparisons.

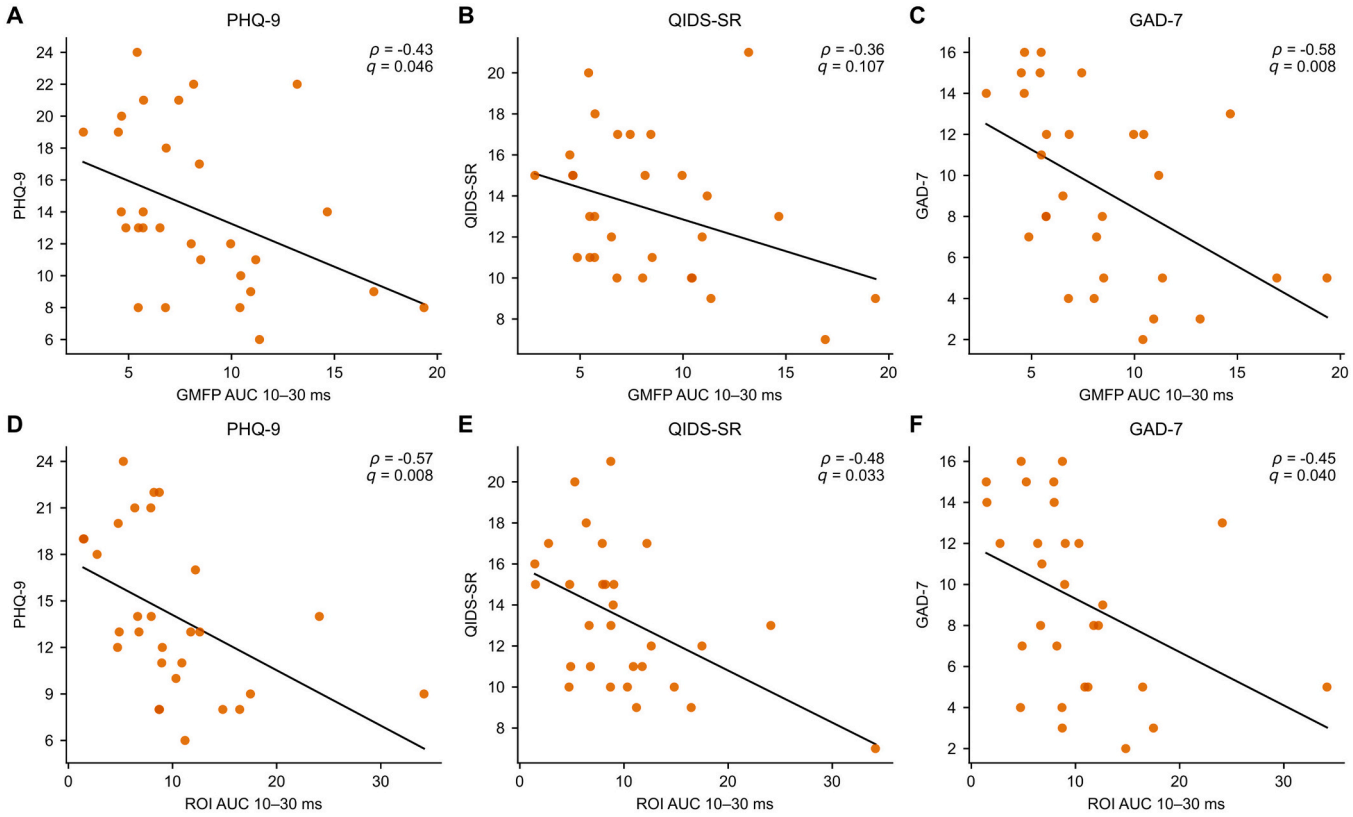


Fig. 3. Associations between early cortical activity and clinical symptom severity following individualized mapped LDLPFC stimulation. Scatter plots show the relationships between early TEP AUC measures recorded during individualized mapped LDLPFC stimulation and clinical symptom severity in participants with MDD. Top row: associations between **GMFP AUC measured over 10–30 ms** and PHQ-9 (A), QIDS-SR (B), and GAD-7 (C) scores. Bottom row: corresponding associations for the **LDLPFC ROI AUC measured over 10–30 ms** and PHQ-9 (D), QIDS-SR (E), and GAD-7 (F) scores. Points represent individual participants, and solid lines indicate least-squares regression fits for visualization. Statistical annotations show Spearman correlation coefficients (ρ) and Benjamini–Hochberg false discovery rate (FDR)-corrected *q*-values from the corresponding correlation analyses.

Table 4
Associations between AUC-based measures of early cortical activity and clinical symptom severity. Spearman correlation coefficients (ρ) between TMS–EEG area-under-the-curve (AUC) measures and clinical symptom scores in participants with major depressive disorder (MDD) are shown for individualized mapped left dorsolateral prefrontal cortex (LDLPFC) stimulation and conventional Beam F3 targeting. Early (10–30 ms) and later (30–80 ms) cortical activity were quantified using global mean field power (GMFP) and left DLPFC region-of-interest (ROI) AUC measures. Correlations are reported with Benjamini–Hochberg false discovery rate (FDR)-corrected *q*-values calculated within the AUC correlation family. Asterisks indicate statistically significant associations after FDR correction ($q < 0.05$).

Metric	Target	PHQ-9	QIDS-SR	GAD-7
GMFP AUC 10–30 ms	Mapped LDLPFC	ρ = –0.43 (q = 0.046)*	ρ = –0.36 (q = 0.107)	ρ = –0.58 (q = 0.008)*
	Beam F3	ρ = –0.01 (q = 0.968)	ρ = –0.01 (q = 0.968)	ρ = 0.01 (q = 0.968)
ROI AUC 10–30 ms	Mapped LDLPFC	ρ = –0.57 (q = 0.008)*	ρ = –0.48 (q = 0.033)*	ρ = –0.45 (q = 0.040)*
	Beam F3	ρ = –0.13 (q = 0.968)	ρ = –0.07 (q = 0.968)	ρ = –0.03 (q = 0.968)
GMFP AUC 30–80 ms	Mapped LDLPFC	ρ = –0.06 (q = 0.840)	ρ = –0.15 (q = 0.655)	ρ = 0.01 (q = 0.972)
	Beam F3	ρ = –0.17 (q = 0.968)	ρ = –0.07 (q = 0.968)	ρ = 0.03 (q = 0.968)
ROI AUC 30–80 ms	Mapped LDLPFC	ρ = –0.20 (q = 0.531)	ρ = –0.13 (q = 0.655)	ρ = 0.08 (q = 0.831)
	Beam F3	ρ = –0.12 (q = 0.968)	ρ = –0.06 (q = 0.968)	ρ = 0.14 (q = 0.968)

Table 5
Partial correlations between early cortical activity and clinical symptom severity controlling for later cortical responses. Partial Spearman correlation coefficients (ρ) between early (10–30 ms) TMS–EEG area-under-the-curve (AUC) measures and clinical symptom scores in participants with major depressive disorder (MDD) are shown after controlling for later cortical activity (30–80 ms) within the same signal representation. Analyses were performed separately for global mean field power (GMFP) and left dorsolateral prefrontal cortex (LDLPFC) region-of-interest (ROI) AUC measures obtained during individualized mapped stimulation and conventional Beam F3 targeting. Benjamini–Hochberg false discovery rate (FDR)-corrected *q*-values were calculated within the partial correlation family. Asterisks indicate statistically significant associations after FDR correction ($q < 0.05$).

Metric	Target	Covariate	PHQ-9	QIDS-SR	GAD-7
GMFP AUC 10–30 ms	Mapped LDLPFC	GMFP AUC 30–80 ms	ρ = –0.43 (q = 0.024)*	ρ = –0.36 (q = 0.058)	ρ = –0.58 (q = 0.003)*
	Beam F3	GMFP AUC 30–80 ms	ρ = 0.20 (q = 0.913)	ρ = 0.07 (q = 0.913)	ρ = –0.02 (q = 0.913)
ROI AUC 10–30 ms	Mapped LDLPFC	ROI AUC 30–80 ms	ρ = –0.63 (q = 0.002)*	ρ = –0.52 (q = 0.008)*	ρ = –0.45 (q = 0.022)*
	Beam F3	ROI AUC 30–80 ms	ρ = –0.07 (q = 0.913)	ρ = –0.05 (q = 0.913)	ρ = –0.16 (q = 0.913)

4. Discussion

The principal finding of this study is that stimulation target selection substantially influences the measurement of early TMS–EEG responses from the left DLPFC. Individualized mapping produced significantly different early TMS-evoked responses than Beam F3 stimulation across both regional (ROI) and global (GMFP) measures. Only individualized mapping consistently identified associations between reduced early cortical activity and greater depressive and anxiety symptom severity. These associations remained significant after controlling for later cortical activity, indicating that clinically relevant information is contained within the earliest phase of the cortical response.

We developed individualized mapping to address several limitations of conventional DLPFC stimulation. Standard targeting relies on scalp landmarks and stimulation intensities are derived from motor cortex physiology, despite substantial inter-individual variability in head anatomy, cortical morphology (Mueller et al., 2013; Zilles et al., 1997), scalp-to-cortex distance (Stokes et al., 2005), and local cortical responsiveness (Ziemann, 2026). These sources of variability can reduce early cortical responses and increase stimulation-related artifacts. Consistent with our previous methodological work (Ukharova et al., 2025), individualized mapping produced substantially different early TEP profiles than Beam F3 targeting, indicating that stimulation location, orientation, and intensity strongly influence the measurable cortical response (Gogulski et al., 2024a,b).

An additional observation was the substantial interindividual variability in the stimulation intensity required to obtain robust early DLPFC responses. Whereas Beam F3 stimulation was delivered at a fixed intensity of 120% RMT, the optimal intensity identified by individualized mapping ranged from 80% to 213% RMT, with approximately two-thirds of participants receiving lower stimulation intensities and one-third requiring higher intensities. Furthermore, individualized stimulation intensity was strongly inversely associated with resting motor threshold, indicating that motor threshold does not reliably predict the stimulation intensity required to evoke robust early responses in the prefrontal cortex. This finding is consistent with previous evidence that motor cortex excitability cannot be assumed to reflect excitability of non-motor cortical regions and further supports individualized optimization of stimulation parameters for TMS–EEG studies targeting the DLPFC (Casula et al., 2018; Krile et al., 2023; Peterchev et al., 2012; Siebner et al., 2022; Stokes et al., 2005).

Individualized mapping also reduced residual muscle activity compared with Beam F3 stimulation. Cranial muscle activation overlaps with the latency of the earliest cortical responses and is therefore a major challenge when quantifying early TMS–EEG signals (Mutanen et al., 2016). Although identical preprocessing was applied to both conditions, residual muscle activity remained greater with Beam F3 stimulation. This suggests that target selection influences not only cortical activation but also signal quality. The improved clinical sensitivity of the individualized mapping is therefore likely explained by a combination of stronger engagement of the target cortex and reduced contamination of early TMS–EEG responses by muscle activity (Casarotto et al., 2022).

The effects of target selection extended beyond response amplitude. Individualized mapping consistently produced smaller early AUC values than Beam F3 stimulation for both GMFP and ROI signals. Several canonical TEP components (N15, P30, and N45) also differed between targeting approaches. These findings indicate that individualized mapping changes the temporal profile of the evoked response rather than simply its overall magnitude. Similar effects have been reported previously, with relatively small changes in stimulation parameters producing substantial differences in TMS-evoked responses (Casarotto et al., 2010; de Goede et al., 2018; Lioumis et al., 2025). Such differences likely reflect variation in local neuronal properties (Harquel et al., 2016), as well as conductivity profiles shaping the stimulating fields (Janssen et al., 2014; Thielscher et al., 2011).

Importantly, clinically relevant information was captured by integrated measures of early cortical activity rather than by conventional TEP peaks. Lower early GMFP AUC was associated with greater depression and anxiety symptom severity, whereas lower early ROI AUC showed robust associations with depressive symptoms measured using both PHQ-9 and QIDS-SR as well as anxiety severity. None of these associations were observed with Beam F3 stimulation. Moreover, the associations remained significant after controlling for later cortical activity (30–80 ms), indicating that they specifically reflect the earliest cortical response rather than overall response magnitude.

Regional and global measures also appeared to capture partly different aspects of symptomatology. ROI AUC showed the strongest

associations with depressive symptoms, whereas GMFP AUC was more strongly associated with anxiety symptoms. While these findings require replication, they may reflect complementary physiological processes. ROI signals primarily represent activity near the stimulation site, whereas GMFP summarizes activity across the scalp and may be more sensitive to the early propagation of cortical activity through distributed networks (Cruciani et al., 2023; Ziemann, 2026).

Our results also provide a different perspective on previous TMS–EEG biomarker studies in depression. Most previous studies have focused on individual TEP components such as N45, P60, and N100 (Cao et al., 2021; Kallioniemi and Daskalakis, 2022; Sun et al., 2018, 2016). In the present work, the conventional peak-based TEP measures showed comparatively limited clinical sensitivity. Although individualized mapping significantly altered several canonical peak amplitudes and latencies relative to Beam F3 stimulation, only P60 latency demonstrated a significant correlation with symptom severity after correction for multiple comparisons. This might be attributed to the nature of the peak-based measures, which heavily depend on reliable identification of individual extrema and are sensitive to noise, preprocessing choices (Bertazzoli et al., 2021), and inter-individual variability in waveform morphology (Ozdemir et al., 2021). By integrating activity across predefined physiological time windows, AUC measures provide a more stable description of early cortical activation that does not depend on accurate identification of individual extrema. The stronger and more consistent clinical associations observed for AUC measures therefore support the use of integrated early-response metrics as candidate biomarkers for TMS–EEG studies.

Despite strong symptom-related associations, none of the early AUC measures differed significantly between participants with MDD and healthy controls after correction for multiple comparisons. Early GMFP AUC showed a moderate effect size but did not survive FDR correction. This suggests that early cortical responses may vary continuously with symptom severity rather than reflecting a categorical diagnostic marker. It is consistent with evidence that neurophysiological measures better capture dimensional variation in psychiatric symptoms than diagnostic categories alone (Drysdale et al., 2017; Insel et al., 2010).

The physiological mechanisms underlying reduced early cortical responses remain uncertain. The earliest TMS-evoked responses are thought to reflect direct activation of superficial pyramidal neurons and the initial recruitment of local excitatory and inhibitory circuits before substantial sensory contributions (Casarotto et al., 2022; Conde et al., 2019; Ziemann, 2026). Reduced early AUC may therefore reflect diminished cortical responsiveness, altered excitation–inhibition balance, or impaired recruitment of local cortical populations. The partially distinct associations observed for ROI and GMFP measures further suggest that local activation and its early propagation through cortical networks may contribute differently to depressive and anxiety symptoms. Future studies combining TMS–EEG with reliable real-time artifact rejection, source reconstruction, electric-field modeling, pharmacological interventions, and computational modeling will be needed to clarify these mechanisms.

Several limitations should be considered. First, the sample size was modest, particularly for the healthy control group, limiting statistical power for detecting diagnostic group differences. Second, the patient cohort was clinically heterogeneous with respect to medication use and comorbidities, which may have increased neurophysiological variability. Third, the cross-sectional design precludes conclusions regarding causality or treatment responsiveness. Longitudinal studies will be necessary to determine whether the early responses change with symptom improvement and whether they predict clinical outcome.

An additional methodological consideration is that individualized mapping explicitly optimized stimulation parameters to maximize early cortical responses while minimizing stimulation-related artifacts. Consequently, the observed improvements likely reflect both more effective engagement of the targeted cortex and higher-quality EEG recordings. Although the AUC measures themselves were not optimized during target selection, they remain dependent on the overall strength of the evoked response. Future work should therefore evaluate whether similar clinical associations are obtained using independently selected stimulation sites, automated optimization procedures, and prospective validation cohorts.

The present study also did not assess test–retest reliability. One motivation for developing AUC-based measures was their reduced dependence on peak identification, which is particularly susceptible to noise, latency variability, and preprocessing choices. Future work should directly compare the reliability of AUC-based and conventional peak-based measures across repeated recording sessions and alternative preprocessing pipelines.

Finally, although individualized TMS–EEG mapping currently requires additional acquisition time and operator expertise, ongoing developments in EEG-guided optimization (Granö et al., 2025; Parmigiani et al., 2025; Tervo et al., 2022), electric-field modeling (Soto et al., 2026), and multi-locus TMS (Matsuda et al., 2025; Nieminen et al., 2022; Sinisalo et al., 2024) are expected to provide more automated and reproducible optimization procedures.

5. Conclusions

Individualized TMS–EEG mapping substantially altered the measurement of early DLPFC responses, reduced residual muscle contamination, and revealed associations between early cortical activity and clinical symptom severity that were not detectable using conventional Beam F3 targeting. Integrated AUC measures of the earliest cortical response demonstrated stronger and more consistent clinical associations than conventional TMS-evoked potential peak measures. Early ROI AUC was associated with depressive symptom severity, whereas early GMFP AUC showed the strongest association with anxiety symptoms. Importantly, these relationships remained significant after controlling for later cortical activity, indicating that clinically relevant information is contained specifically within the earliest phase of the cortical response rather than reflecting overall response magnitude. These findings highlight the importance of individualized stimulation targeting and signal quality for measuring early TMS–EEG responses and support early AUC-based measures as promising biomarkers of symptom-related cortical dysfunction. Future longitudinal and treatment studies are needed to establish their reliability, predictive value, and clinical utility.

6. Disclosures

PL is a consultant to Nexstim Plc for TMS–EEG applications and speech cortical mapping. RJI has patents on TMS technology, has consulted Nexstim Plc on TMS, and is co-founder and shareholder of Cortisys Ltd. ZJD has received research and equipment in-kind support for an investigator-initiated study through Brainsway Inc and Magventure Inc. He also currently serves on the scientific advisory board for Brainsway Inc. His work has been supported by the National Institutes of Mental Health (NIMH), the Canadian Institutes of Health Research (CIHR), Brain Canada and the Temerty Family, Grant and Kreutzkamp Family Foundations, and the Wellcome Foundation. DMB receives research support from CIHR, NIMH, Wellcome Trust, Brain Canada and the Temerty Family through the CAMH Foundation and the Campbell Family Research Institute, has received research grant support and in-kind equipment support for an investigator-initiated study from Brainsway Ltd, was the site principal investigator for three sponsor-initiated studies for Brainsway Ltd, has received in-kind equipment support from Magventure for investigator-initiated studies, has received medication supplies for an investigator-initiated trial from Indivior, is a scientific advisor for Sooma Medical and is a member of the Clinical Standards Committee of the Clinical TMS Society (unpaid). EU, IO, IG, SS, EI, CT, NK, PP, MV, SP, JMP, TR, JG report no potential conflicts of interest.

Acknowledgements

We would like to acknowledge the contribution of the MDD patients and healthy volunteers that led to the development of our experimental protocol.

This work was supported by Wellcome Leap, United States, as part of the Multi-Channel Psych Program. This project has also received funding from the European Research Council (ERC) under the European Union's Horizon 2020 Research and Innovation Programme (grant agreement No 81037). JG has received a personal grant from Emil Aaltonen Foundation, Finland and Young Group Leaders Grant from Sigrid Juselius Foundation, Finland, supporting work of JG and CT.

Appendix A. Supplementary material

Supplementary data to this article can be found online at https://doi.org/10.1016/j.clinph.2026.2112427.

References

Ahdab, R., Ayache, S.S., Brugières, P., Goujon, C., Lefaucheur, J.-P., 2010. Comparison of "standard" and "navigated" procedures of TMS coil positioning over motor, premotor and prefrontal targets in patients with chronic pain and depression. Neurophysiol. Clin. Clin. Neurophysiol. 40, 27–36. https://doi.org/10.1016/j.neucli.2010.01.001.

Awiszus, F., 2003. TMS and threshold hunting. Suppl. Clin. Neurophysiol. 56, 13–23. https://doi.org/10.1016/s1567-424x(09)70205-3.

Aydogan, D.B., Souza, V.H., Matsuda, R.H., Lioumis, P., Ilmoniemi, R.J., 2023. In: Real-Time Tractography-Assisted Neuronavigation for TMS, 531565. https://doi.org/10.1101/2023.03.09.531565.

Beam, W., Borckardt, J.J., Reeves, S.T., George, M.S., 2009. An efficient and accurate new method for locating the F3 position for prefrontal TMS applications. Brain Stimulat. 2, 50–54. https://doi.org/10.1016/j.brs.2008.09.006.

Bertazzoli, G., Esposito, R., Mutanen, T.P., Ferrari, C., Ilmoniemi, R.J., Miniussi, C., et al., 2021. The impact of artifact removal approaches on TMS–EEG signal. Neuroimage 239, 118272. https://doi.org/10.1016/j.neuroimage.2021.118272.

Biermann, L., Wunram, H.L., Pokorny, L., Breitinger, E., Großheinrich, N., Jarczok, T.A., et al., 2022. Changes in the TMS-evoked potential N100 in the dorsolateral prefrontal cortex as a function of depression severity in adolescents. J. Neural Transm. 129, 1339–1352. https://doi.org/10.1007/s00702-022-02539-9.

Cao, K.-X., Ma, M.-L., Wang, C.-Z., Iqbal, J., Si, J.-J., Xue, Y.-X., et al., 2021. TMS-EEG: an emerging tool to study the neurophysiologic biomarkers of psychiatric disorders. Neuropharmacology 197, 108574. https://doi.org/10.1016/j.neuropharm.2021.108574.

Casali, A.G., Casarotto, S., Rosanova, M., Mariotti, M., Massimini, M., 2010. General indices to characterize the electrical response of the cerebral cortex to TMS. Neuroimage 49, 1459–1468. https://doi.org/10.1016/j.neuroimage.2009.09.026.

Casarotto, S., Fecchio, M., Rosanova, M., Varone, G., D'Ambrosio, S., Sarasso, S., et al., 2022. The rt-TEP tool: real-time visualization of TMS-evoked potentials to maximize cortical activation and minimize artifacts. J. Neurosci. Methods 370, 109486. https://doi.org/10.1016/j.jneumeth.2022.109486.

Casarotto, S., Romero Lauro, L.J., Bellina, V., Casali, A.G., Rosanova, M., Pigorini, A., et al., 2010. EEG responses to TMS are sensitive to changes in the perturbation parameters and repeatable over time. PLoS One 5, e10281. https://doi.org/10.1371/journal.pone.0010281.

Cash, R.F.H., Cocchi, L., Lv, J., Wu, Y., Fitzgerald, P.B., Zalesky, A., 2021. Personalized connectivity-guided DLPFC-TMS for depression: advancing computational feasibility, precision and reproducibility. Hum. Brain Mapp. 42, 4155–4172. https://doi.org/10.1002/hbm.25330.

Cash, R.F.H., Zalesky, A., 2024. Personalized and circuit-based transcranial magnetic stimulation: evidence, controversies, and opportunities. Biol. Psychiatry 95, 510–522. https://doi.org/10.1016/j.biopsych.2023.11.013.

Casula, E.P., Rocchi, L., Hannah, R., Rothwell, J.C., 2018. Effects of pulse width, waveform and current direction in the cortex: a combined cTMS-EEG study. Brain Stimulat. 11, 1063–1070. https://doi.org/10.1016/j.brs.2018.04.015.

Caulfield, K.A., Li, X., George, M.S., 2021. Four electric field modeling methods of dosing prefrontal transcranial magnetic stimulation (TMS): introducing APEX MT dosimetry. Brain Stimulat. 14, 1032–1034. https://doi.org/10.1016/j.brs.2021.06.012.

Cline, C.C., Lucas, M.V., Sun, Y., Menezes, M., Etkin, A., 2021. Advanced artifact removal for automated TMS-EEG data processing. In: 2021 10th Int. IEEEEMBS Conf. Neural Eng. NER, pp. 1039–1042. https://doi.org/10.1109/NER49283.2021.9441147.

Cole, E.J., Stimpson, K.H., Bentzley, B.S., Gulser, M., Cherian, K., Tischler, C., et al., 2020. Stanford accelerated intelligent neuromodulation therapy for treatment-resistant depression. Am. J. Psychiatry 177, 716–726. https://doi.org/10.1176/appi.ajp.2019.19070720.

Conde, V., Tomasevic, L., Akopian, I., Stanek, K., Saturnino, G.B., Thielscher, A., et al., 2019. The non-transcranial TMS-evoked potential is an inherent source of ambiguity in TMS-EEG studies. Neuroimage 185, 300–312. https://doi.org/10.1016/j.neuroimage.2018.10.052.

Cruciani, A., Mancuso, M., Sveva, V., Maccarrone, D., Todisco, A., Motolese, F., et al., 2023. Using TMS-EEG to assess the effects of neuromodulation techniques: a narrative review. Front. Hum. Neurosci. 17, 1247104. https://doi.org/10.3389/fnhum.2023.1247104.

Darmani, G., Ziemann, U., 2019. Pharmacophysiology of TMS-evoked EEG potentials: a mini-review. Brain Stimulat. 12, 829–831. https://doi.org/10.1016/j.brs.2019.02.021.

Delorme, A., Makeig, S., 2004. EEGLAB: an open source toolbox for analysis of single-trial EEG dynamics including independent component analysis. J. Neurosci. Methods 134, 9–21. https://doi.org/10.1016/j.jneumeth.2003.10.009.

Dhami, P., Atluri, S., Lee, J.C., Knyahnytska, Y., Croarkin, P.E., Blumberger, D.M., et al., 2020. Prefrontal cortical reactivity and connectivity markers distinguish youth depression from healthy youth. Cereb. Cortex. N Y NY 30, 3884–3894. https://doi.org/10.1093/cercor/bhaa004.

Dhami, P., Moreno, S., Croarkin, P.E., Blumberger, D.M., Daskalakis, Z.J., Farzan, F., 2023. Baseline markers of cortical excitation and inhibition predict response to theta burst stimulation treatment for youth depression. Sci. Rep. 13, 19115. https://doi.org/10.1038/s41598-023-45107-1.

Dhiman, S., Hickey, R.E., Thorn, K.E., Moss, H.G., McKinnon, E.T., Adisetiyo, V., et al., 2024. PyDesigner v1.0: a pythonic implementation of the DESIGNER Pipeline for diffusion magnetic resonance imaging. J. Vis. Exp. JoVE. https://doi.org/10.3791/66397.

Drysdale, A.T., Grosenick, L., Downar, J., Dunlop, K., Mansouri, F., Meng, Y., et al., 2017. Resting-state connectivity biomarkers define neurophysiological subtypes of depression. Nat. Med. 23, 28–38. https://doi.org/10.1038/nm.4246.

Eshel, N., Keller, C.J., Wu, W., Jiang, J., Mills-Finnerty, C., Huemer, J., et al., 2020. Global connectivity and local excitability changes underlie antidepressant effects of repetitive transcranial magnetic stimulation. Neuropsychopharmacol. Off. Publ. Am. Coll. Neuropsychopharmacol. 45, 1018–1025. https://doi.org/10.1038/s41386-020-0633-z.

Esteban, O., Markiewicz, C.J., Blair, R.W., Moodie, C.A., Isik, A.I., Erramuzpe, A., et al., 2019. fMRIPrep: a robust preprocessing pipeline for functional MRI. Nat. Methods 16, 111–116. https://doi.org/10.1038/s41592-018-0235-4.

Fox, M.D., Buckner, R.L., White, M.P., Greicius, M.D., Pascual-Leone, A., 2012. Efficacy of transcranial magnetic stimulation targets for depression is related to intrinsic functional connectivity with the subgenual cingulate. Biol. Psychiatry 72, 595–603. https://doi.org/10.1016/j.biopsych.2012.04.028.

Glasser, M.F., Coalson, T.S., Robinson, E.C., Hacker, C.D., Harwell, J., Yacoub, E., et al., 2016. A multi-modal parcellation of human cerebral cortex. Nature 536, 171–178. https://doi.org/10.1038/nature18933.

de Goede, A.A., Ter Braack, E.M., van Putten, M.J.A.M., 2018. Accurate coil positioning is important for single and paired pulse TMS on the subject level. Brain Topogr. 31, 917–930. https://doi.org/10.1007/s10548-018-0655-6.

Gogulski, J., Cline, C.C., Ross, J.M., Parmigiani, S., Keller, C.J., 2024a. Reliability of the TMS-evoked potential in dorsolateral prefrontal cortex. Cereb Cortex N Y N 34, bhae130. https://doi.org/10.1093/cercor/bhae130.

Gogulski, J., Cline, C.C., Ross, J.M., Truong, J., Sarkar, M., Parmigiani, S., et al., 2024b. Mapping cortical excitability in the human dorsolateral prefrontal cortex. Clin. Neurophysiol. 164, 138–148. https://doi.org/10.1016/j.clinph.2024.05.008.

Granö, I., Kahilakoski, O.-P., Laine, M., Kirchhoff, M., Ahola, O., Soto, A.M., et al., 2025. In: Fast and Standardized Motor-Hotspot Determination with Automated TMS Mapping, 678288. https://doi.org/10.1101/2025.09.24.678288.

Harquel, S., Bacle, T., Beynel, L., Marendaz, C., Chauvin, A., David, O., 2016. Mapping dynamical properties of cortical microcircuits using robotized TMS and EEG: towards functional cytoarchitectonics. Neuroimage 135, 115–124. https://doi.org/10.1016/j.neuroimage.2016.05.009.

Hernandez-Pavon, J.C., Kugiumtzis, D., Zrenner, C., Kimiskidis, V.K., Metsomaa, J., 2022. Removing artifacts from TMS-evoked EEG: a methods review and a unifying theoretical framework. J. Neurosci. Methods 376, 109591. https://doi.org/10.1016/j.jneumeth.2022.109591.

Hernandez-Pavon, J.C., Veniero, D., Bergmann, T.O., Belardinelli, P., Bortoletto, M., Casarotto, S., et al., 2023. TMS combined with EEG: recommendations and open issues for data collection and analysis. Brain Stimulat. 16, 567–593. https://doi.org/10.1016/j.brs.2023.02.009.

Ilmoniemi, R.J., Virtanen, J., Ruohonen, J., Karhu, J., Aronen, H.J., Näätänen, R., et al., 1997. Neuronal responses to magnetic stimulation reveal cortical reactivity and connectivity. Neuroreport 8, 3537–3540. https://doi.org/10.1097/00001756-199711100-00024.

Insel, T., Cuthbert, B., Garvey, M., Heinssen, R., Pine, D.S., Quinn, K., et al., 2010. Research domain criteria (RDoC): toward a new classification framework for research on mental disorders. Am. J. Psychiatry 167, 748–751. https://doi.org/10.1176/appi.ajp.2010.09091379.

Janssen, A.M., Oostendorp, T.F., Stegeman, D.F., 2014. The effect of local anatomy on the electric field induced by TMS: evaluation at 14 different target sites. Med. Biol. Eng. Compu. 52, 873–883. https://doi.org/10.1007/s11517-014-1190-6.

Kallioniemi, E., Daskalakis, Z.J., 2022. Identifying novel biomarkers with TMS-EEG - methodological possibilities and challenges. J. Neurosci. Methods 377, 109631. https://doi.org/10.1016/j.jneumeth.2022.109631.

Krile, L., Ensafi, E., Cole, J., Noor, M., Protzner, A.B., McGirr, A., 2023. A dose-response characterization of transcranial magnetic stimulation intensity and evoked potential amplitude in the dorsolateral prefrontal cortex. Sci. Rep. 13, 18650. https://doi.org/10.1038/s41598-023-45730-y.

Leuchter, A.F., Cook, I.A., Hunter, A.M., Korb, A.S., 2009. A new paradigm for the prediction of antidepressant treatment response. Dialogues Clin. Neurosci. 11, 435–446. https://doi.org/10.31887/DCNS.2009.11.4/afleuchter.

Li, X., Honda, S., Nakajima, S., Wada, M., Yoshida, K., Daskalakis, Z.J., et al., 2021. TMS-EEG research to elucidate the pathophysiological neural bases in patients with schizophrenia: a systematic review. J. Pers. Med. 11, 388. https://doi.org/10.3390/jpm11050388.

Lioumis, P., Roine, T., Granö, I., Aydogan, D.B., Ukharova, E., Souza, V.H., et al., 2025. Optimization of TMS target engagement: current state and future perspectives. Front. Neurosci. 19, 1517228. https://doi.org/10.3389/fnins.2025.1517228.

Lioumis, P., Rosanova, M., 2022. The role of neuronavigation in TMS-EEG studies: current applications and future perspectives. J. Neurosci. Methods 380, 109677. https://doi.org/10.1016/j.jneumeth.2022.109677.

Matsuda, R.H., Souza, V.H., Marchetti, T.C., Soto, A.M., Kahilakoski, O.-P., Laine, M., et al., 2025. Characterizing an electronic–robotic targeting platform for precise and fast brain stimulation with multi-locus transcranial magnetic stimulation. Phys. Med. Biol. 70, 165015. https://doi.org/10.1088/1361-6560/adf36e.

Mueller, S., Wang, D., Fox, M.D., Thomas Yeo, B.T., Sepulcre, J., Sabuncu, M.R., et al., 2013. Individual variability in functional connectivity architecture of the human brain. Neuron 77, 586–595. https://doi.org/10.1016/j.neuron.2012.12.028.

Mutanen, T.P., Kukkonen, M., Nieminen, J.O., Stenroos, M., Sarvas, J., Ilmoniemi, R.J., 2016. Recovering TMS-evoked EEG responses masked by muscle artifacts. Neuroimage 139, 157–166. https://doi.org/10.1016/j.neuroimage.2016.05.028.

Mutanen, T.P., Metsomaa, J., Liljander, S., Ilmoniemi, R.J., 2018. Automatic and robust noise suppression in EEG and MEG: the SOUND algorithm. Neuroimage 166, 135–151. https://doi.org/10.1016/j.neuroimage.2017.10.021.

Nieminen, J.O., Sinisalo, H., Souza, V.H., Malmi, M., Yuryev, M., Tervo, A.E., et al., 2022. Multi-locus transcranial magnetic stimulation system for electronically targeted brain stimulation. Brain Stimulat. 15, 116–124. https://doi.org/10.1016/j.brs.2021.11.014.

Oja, E., Yuan, Z., 2006. The fastICA algorithm revisited: convergence analysis. IEEE Trans. Neural Netw. 17, 1370–1381. https://doi.org/10.1109/TNN.2006.880980.

Ozdemir, R.A., Tadayon, E., Boucher, P., Sun, H., Momi, D., Ganglberger, W., et al., 2021. Cortical responses to noninvasive perturbations enable individual brain fingerprinting. Brain Stimulat. 14, 391–403. https://doi.org/10.1016/j.brs.2021.02.005.

Parmigiani, S., Cline, C.C., Sarkar, M., Forman, L., Truong, J., Ross, J.M., et al., 2025. Real-time optimization to enhance noninvasive cortical excitability assessment in the human dorsolateral prefrontal cortex. Clin. Neurophysiol. Off. J. Int. Fed. Clin. Neurophysiol. 174, 225–234. https://doi.org/10.1016/j.clinph.2025.02.261.

Peterchev, A.V., Wagner, T.A., Miranda, P.C., Nitsche, M.A., Paulus, W., Lisanby, S.H., et al., 2012. Fundamentals of transcranial electric and magnetic stimulation dose: definition, selection, and reporting practices. Brain Stimulat. 5, 435–453. https://doi.org/10.1016/j.brs.2011.10.001.

Pion-Tonachini, L., Kreutz-Delgado, K., Makeig, S., 2019. ICLabel: an automated electroencephalographic independent component classifier, dataset, and website. Neuroimage 198, 181–197. https://doi.org/10.1016/j.neuroimage.2019.05.026.

Rogasch, N.C., Sullivan, C., Thomson, R.H., Rose, N.S., Bailey, N.W., Fitzgerald, P.B., et al., 2017. Analysing concurrent transcranial magnetic stimulation and electroencephalographic data: a review and introduction to the open-source TESA software. Neuroimage 147, 934–951. https://doi.org/10.1016/j.neuroimage.2016.10.031.

Russo, S., Sarasso, S., Puglisi, G.E., Dal Palù, D., Pigorini, A., Casarotto, S., et al., 2022. TAAC - TMS adaptable auditory control: a universal tool to mask TMS clicks. J. Neurosci. Methods 370, 109491. https://doi.org/10.1016/j.jneumeth.2022.109491.

Siddiqi, S.H., Weigand, A., Pascual-Leone, A., Fox, M.D., 2021. Identification of personalized transcranial magnetic stimulation targets based on subgenual cingulate connectivity: an independent replication. Biol. Psychiatry 90, e55–e56. https://doi.org/10.1016/j.biopsych.2021.02.015.

Siebner, H.R., Funke, K., Aberra, A.S., Antal, A., Bestmann, S., Chen, R., et al., 2022. Transcranial magnetic stimulation of the brain: what is stimulated? – A consensus and critical position paper. Clin. Neurophysiol. 140, 59–97. https://doi.org/10.1016/j.clinph.2022.04.022.

Sinisalo, H., Rissanen, I., Kahilakoski, O.-P., Souza, V.H., Tommila, T., Laine, M., et al., 2024. Modulating brain networks in space and time: Multi-locus transcranial magnetic stimulation. Clin. Neurophysiol. Off. J. Int. Fed. Clin. Neurophysiol. 158, 218–224. https://doi.org/10.1016/j.clinph.2023.12.007.

Soto, A.M., Stenroos, M., Matsuda, R.H., Mylläri, T., Jyrkinen, K., Sinisalo, H., et al., 2026. Real-time electric-field neuronavigation on realistic head models for conventional and multi-locus TMS. Brain Stimulat 19, 103113. https://doi.org/10.1016/j.brs.2026.103113.

Stokes, M.G., Chambers, C.D., Gould, I.C., Henderson, T.R., Janko, N.E., Allen, N.B., et al., 2005. Simple metric for scaling motor threshold based on scalp-cortex distance: application to studies using transcranial magnetic stimulation. J. Neurophysiol. 94, 4520–4527. https://doi.org/10.1152/jn.00067.2005.

Sun, Y., Blumberger, D.M., Mulsant, B.H., Rajji, T.K., Fitzgerald, P.B., Barr, M.S., et al., 2018. Magnetic seizure therapy reduces suicidal ideation and produces neuroplasticity in treatment-resistant depression. Transl. Psychiatry 8, 253. https://doi.org/10.1038/s41398-018-0302-8.

Sun, Y., Farzan, F., Mulsant, B.H., Rajji, T.K., Fitzgerald, P.B., Barr, M.S., et al., 2016. Indicators for remission of suicidal ideation following magnetic seizure therapy in patients with treatment-resistant depression. JAMA Psychiat. 73, 337–345. https://doi.org/10.1001/jamapsychiatry.2015.3097.

Tervo, A.E., Nieminen, J.O., Lioumis, P., Metsomaa, J., Souza, V.H., Sinisalo, H., et al., 2022. Closed-loop optimization of transcranial magnetic stimulation with electroencephalography feedback. Brain Stimulat 15, 523–531. https://doi.org/10.1016/j.brs.2022.01.016.

Thielscher, A., Opitz, A., Windhoff, M., 2011. Impact of the gyral geometry on the electric field induced by transcranial magnetic stimulation. Neuroimage 54, 234–243. https://doi.org/10.1016/j.neuroimage.2010.07.061.

Tournier, J.-D., Smith, R., Raffelt, D., Tabbara, R., Dhollander, T., Pietsch, M., et al., 2019. MRtrix3: a fast, flexible and open software framework for medical image processing and visualisation. Neuroimage 202, 116137. https://doi.org/10.1016/j.neuroimage.2019.116137.

Tremblay, S., Rogasch, N.C., Premoli, I., Blumberger, D.M., Casarotto, S., Chen, R., et al., 2019. Clinical utility and prospective of TMS-EEG. Clin. Neurophysiol. Off. J. Int. Fed. Clin. Neurophysiol. 130, 802–844. https://doi.org/10.1016/j.clinph.2019.01.001.

Trivedi, M.H., Rush, A.J., Wisniewski, S.R., Nierenberg, A.A., Warden, D., Ritz, L., et al., 2006. Evaluation of outcomes with citalopram for depression using measurement-based care in STAR*D: implications for clinical practice. Am. J. Psychiatry 163, 28–40. https://doi.org/10.1176/appi.ajp.163.1.28.

Ukharova, E., Sathyan, S., Granö, I., O'Meeghan, I., Ahola, O., Kainulainen, N., et al., 2025. Neuroimaging-guided TMS-EEG for real-time cortical network mapping. J. Vis. Exp. JoVE. https://doi.org/10.3791/67339.

Voineskos, D., Blumberger, D.M., Zomorrodi, R., Rogasch, N.C., Farzan, F., Foussias, G., et al., 2019. Altered transcranial magnetic stimulation-electroencephalographic markers of inhibition and excitation in the dorsolateral prefrontal cortex in major depressive disorder. Biol. Psychiatry 85, 477–486. https://doi.org/10.1016/j.biopsych.2018.09.032.

Weigand, A., Horn, A., Caballero, R., Cooke, D., Stern, A.P., Taylor, S.F., et al., 2018. Prospective validation that subgenual connectivity predicts antidepressant efficacy of transcranial magnetic stimulation sites. Biol. Psychiatry 84, 28–37. https://doi.org/10.1016/j.biopsych.2017.10.028.

Ziemann, U., Bai, Y., Baumer, F.M., Beck, M.M., Belardinelli, P., Belvisi, D., et al., 2026. Clinical utility and prospective of TMS–EEG: Updated review from an international expert group. Clin. Neurophysiol., 2111487 https://doi.org/10.1016/j.clinph.2025.2111487.

Zilles, K., Schleicher, A., Langemann, C., Amunts, K., Morosan, P., Palomero-Gallagher, N., et al., 1997. Quantitative analysis of sulci in the human cerebral cortex: development, regional heterogeneity, gender difference, asymmetry, intersubject variability and cortical architecture. Hum. Brain Mapp. 5, 218–221. https://doi.org/10.1002/(SICI)1097-0193(1997)5:4%3C218::AID-HBM2%3E3.0.CO;2-6.